

RSC Advances



This is an *Accepted Manuscript*, which has been through the Royal Society of Chemistry peer review process and has been accepted for publication.

Accepted Manuscripts are published online shortly after acceptance, before technical editing, formatting and proof reading. Using this free service, authors can make their results available to the community, in citable form, before we publish the edited article. This *Accepted Manuscript* will be replaced by the edited, formatted and paginated article as soon as this is available.

You can find more information about *Accepted Manuscripts* in the [Information for Authors](#).

Please note that technical editing may introduce minor changes to the text and/or graphics, which may alter content. The journal's standard [Terms & Conditions](#) and the [Ethical guidelines](#) still apply. In no event shall the Royal Society of Chemistry be held responsible for any errors or omissions in this *Accepted Manuscript* or any consequences arising from the use of any information it contains.

ARTICLE

Hierarchical nanostructured polypyrrole/graphene composites as supercapacitor electrode

Cite this: DOI: 10.1039/x0xx00000x

Xin Fan^{*}, Zhewei Yang, Nan HeReceived 00th August 2014,
Accepted 00th August 2014

DOI: 10.1039/x0xx00000x

www.rsc.org/

The electrode composites composed of conductive polypyrrole and graphene for electrochemical capacitors have attracted extensive attentions due to their potential application. Here a green synthesis method was used to fabricate hierarchical nanostructured polypyrrole/graphene composites by using vitamin C as reducing agent. The as-prepared nanocomposites were characterized by FTIR, Raman, XRD, TGA, SEM and TEM techniques. The results showed that the polypyrrole chains in PPy/rGO-CTAB composite successfully inserted into the two-dimensional space of graphene layers. In addition, the electrochemical performances of composites were measured with cyclic voltammetry (CV), galvanostatic charge-discharge (GCD) and electrochemical impedance spectroscopy (EIS) experiments. The results indicated that PPy/rGO-CTAB composites possessed better thermal stability, higher specific capacitance, lower resistance, relatively higher cyclic property and faster response to oxidation/reduction than both PPy/rGO composites without addition of CTAB and rGO.

1 Introduction

Electrochemical capacitors (ECs), as promising efficient electrical energy storage devices, have recently received a keen interest because of their advantages such as high power density, low maintenance cost and long durability in comparison to batteries and conventional capacitors^[1,2]. Further, the investigation in ECs has focused on high performance of electrode with high capacitance, high conductivity and excellent electrochemical cycle stability.

Graphene, a kind of new carbon-based material with 2-D nanostructure^[3], has recently been proposed for potential applications in the field of ECs owing to its exceptional thermal stability, large surface area, outstanding mechanical strength and extremely high electrical conductivity^[4-5]. However, the disadvantage of low capacitance and stack hinders the application in electrochemical capacitors.

Polypyrrole (PPy), as a kind of traditional conducting polymer^[6,7], can be found in the field of storage energy ascribed to low cost, high pseudocapacitance, excellent chemical and environmental stability, and unique conductive mechanism. Nevertheless, the volume expansion induced by doping and dedoping in the electrochemical progress lowers the stability of electrochemical capacitors.

Nowadays, much effort has been devoted to prepare the composites of PPy and graphene which possess not only large surface area, high conductivity and great mechanical property of graphene, but also high pseudocapacitance of PPy.

Sudhakar et al^[8] synthesized graphene oxide(GO)/multilayer nano-PPy structure composite by galvanostatic method, the specific capacitance of which is as high as 332 F/g at 10 mV/s and also

compared with another supercapacitor made from single GO/PPy layer whose capacitance is 215 F/g. Xu et al^[9] fabricated novel hierarchical nanosheet composites(GNS/PPy) which exhibited large electrochemical capacitance (318.6 F/g) at a scan rate of 2 mV/s. Fan et al^[10] prepared PPy/CGN composites via in situ oxidative polymerization of pyrrole in the presence of CTAB intercalated graphene. Biswas et al^[11] combined the nanostructured conductive PPy with highly electrically conductive graphene nanosheets in a multilayered configuration to achieve high specific capacitance and low electronic resistance for supercapacitor electrode applications. However, among these methods, the reducing agent is unfriendly to the environment, and the graphene is first prepared by reduction of graphene oxide followed with polymerization of pyrrole, leading to the agglomeration of graphene again.

The present work demonstrates a green synthetic route to prepare hierarchical nanostructured PPy/reduced GO (PPy/rGO) composite using green vitamin C as reducing agent. Vitamin C is an important environmentally-friendly and low-cost biological molecule, especially its excellent reduction performance. At first, polypyrrole was formed firstly on the surface of GO modified by CTAB (GO-CTAB), and then the PPy/GO-CTAB composites were reduced by vitamin C, avoiding the agglomeration of rGO efficiently. The as-prepared nanocomposites were characterized by Fourier transform infrared spectrometer (FTIR), Raman spectra, X-ray diffractometer (XRD), thermogravimetric analysis (TGA), scanning electron microscopy (SEM) and transmission electron microscope (TEM) techniques. In addition, the electrochemical performances of the as-prepared materials were conducted with a three-electrode cell.

2 Materials and methods

2.1 Materials

Graphite powder and pyrrole were purchased from Aladdin. Sulphuric acid, phosphoric acid, potassium permanganate (KMnO₄), ammonium persulfate (APS), cetyltrimethylammonium bromide, hydrochloric acid, hydrogen peroxide and vitamin C were purchased from Xilong Chemical Corporation Limited (Shantou, China). Absolute alcohol was purchased from Guangdong Guanghua Sci-Tech Co., Ltd (Shantou, China). All reagents were of analytical grade and the pyrrole was distilled before use.

2.2 Preparation of GO

GO was prepared from natural graphite powder by modified Hummers method^[12]. A typical experiment procedure is given below.

Briefly, 3 g of graphite powder was preliminarily treated in oxidizing by adding into 300 mL of mixed acid with concentrated sulfuric acid (H₂SO₄) and phosphoric acid (H₃PO₄) (volume ratio of H₂SO₄: H₃PO₄=9:1) under vigorous agitation for 30 min. 18 g of KMnO₄ was added into the mixture under stirring for 20 min, and the temperature of reaction system was kept under 35 °C, which promoted the depth oxidation of GO. After that, the reaction mixture reacted at the temperature of 50 °C for 12 h. Next, 200 mL deionized water was added into the pasty solution under constant stirring, and the temperature was raised to 80 °C. After vigorous stirring for 2 h, 15 mL of 30% H₂O₂ was added to remove the excess KMnO₄, and the colour of mixture turned golden yellow immediately. Then the reaction mixture was washed in turn by centrifuge with deionized water, 5% HCl and absolute alcohol for several times until the resulting mixture was neutral. Finally, the acquired brown gelatum was centrifuged and dried in vacuum oven at 50 °C overnight.

2.3 Preparation of PPy/rGO nanostructure composite

GO is modified by a kind of cationic surfactant named cetyltrimethylammonium bromide (CTAB) which can lower the surface tension and surface energy of GO, facilitating massive pyrrole monomers to gather on the surface of GO nanosheets and interact with GO via π - π stacking. Then pyrrole monomer micelles are polymerized on the condition of APS^[13]. Finally, the PPy/GO is reduced by mild and green vitamin C. A typical experiment process is shown as follows.

10 mg of graphite oxide and 25 mg of CTAB (mass ratio of CTAB:pyrrole=1:4) were dispersed into 50 mL deionized water with sonication for 2 h. Then 0.1 mL of pyrrole monomer (a constant amount for all the samples) and 2 mL of 1 M HCl were added and stirred for 1 h in ice-water bath, yielding a homogeneous suspension with colour of brown. Next, 30 mL of 0.34 g aqueous solution of APS (mole ratio of pyrrole:APS=1:1) was added drop by drop into the reaction mixture under vigorous agitation in the ice-water bath for 12 h. Afterwards, 20 mL aqueous solution of 1 g vitamin C was added into the resulting precipitate to chemically reduce the PPy/GO-CTAB (GO modified by CTAB) composite for 6 h. Finally, the PPy/rGO-CTAB composite was filtered out and washed with a mount of deionized water until the filtrate was neutral, and dried in an oven at 60 °C.

For comparison, the pure rGO, PPy and PPy/rGO composite without the presence of CTAB were prepared by the same method.

2.4 Material characterization

FTIR was carried out on Fourier transform infrared spectrometer (Thermo Nexus 470 FI-TR). Scanning electron microscopy (SEM) was performed on a Hitachi S4800 FESEM and transmission electron microscopy (TEM) was carried out using a JEOL JEM-2100 TEM operating at an acceleration voltage of 100 kV. The X-ray diffraction patterns of samples were performed on X-ray diffractometer (X'Pert PRO) using Cu-K α radiation in θ -2 θ scans and grazing incidence 2θ scans. Thermal gravimetric analysis (TGA) was measured by a NETZSCH STA 449C analyzer at a heating rate of 10 °C/min in N₂ flow. Raman spectra were performed on DXR Raman Microscope (Thermo Fisher Scientific DXR) using a 532 nm laser under ambient conditions.

2.5 Electrode preparation and electrochemical measurement

The electrochemical measurements were performed on CHI690 electrochemical workstation in an electrolyte of 1 M H₂SO₄ solution, using platinum foil as a counter electrode and saturated calomel electrode as a reference electrode by cyclic voltammetry (CV), galvanostatic charge-discharge (GCD) and electrochemical impedance spectroscopy (EIS) experiments. The specific capacitance of the electrode was measured by GCD and could be calculated according to the following equation:

$$C = I \times \frac{\Delta t}{m} \times \Delta V \quad (1)$$

where I is the current, Δt is the discharge time, m is total mass of active material in a single electrode, and ΔV is the potential window.

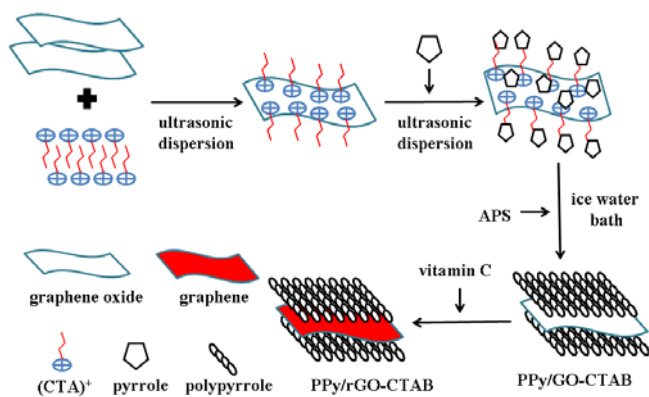
The working electrode was prepared by sufficient mixing the composite, conductive black and polytetrafluor-ethylene (mass ratio=8:1:1), yielding homogeneous slurry under ultrasonic dispersion. The slurry was coated and pressed onto stainless steel wire (the area is 1 cm² and the mass of active material was about 5–10 mg), then dried in a vacuum oven at 60 °C for 24 h.

3 Results and discussion

3.1 Synthesis mechanism of PPy/rGO-CTAB composites

The preparation process of PPy/rGO-CTAB composites is illustrated in Scheme 1. CTAB in aqueous solution is ionized to form quaternary ammonium cation. The GO with negative charge could adsorb the cation of CTAB by electronic interaction, which causes the remaining carbochain of CTAB to stretch out of GO layers. On the basis of similar compatible principle, the carbochains interact with a great deal of pyrrole monomers, which benefits stronger intermolecular force between pyrrole and GO-CTAB. In addition, CTAB, as a surfactant, could lower the surface tension and surface energy of GO, facilitating more pyrrole monomers to gather on the surface of GO via π - π stacking. After the addition of APS, lamellar mesostructural (CTA)₂S₂O₈ is formed due to the interaction between surfactant cations and oxidizing anions, which could be used as a template for the formation of chain-structure polypyrrole^[13]. After complete polymerization, (CTA)₂S₂O₈ would degrade leaving behind the chain-structure polypyrrole. Then the PPy/GO-CTAB is reduced to synthesize the PPy/rGO-CTAB

composites by vitamin C under a mild condition^[14]. The agglomeration of rGO in composites could be efficiently encumbered due to the insertion of the chain-structure PPy into the interlayer of the rGO.



Scheme 1 Preparation of PPy/rGO-CTAB composites.

3.2 IR analysis

The FTIR spectra of GO, PPy, PPy/rGO and PPy/rGO-CTAB composites are presented in Fig.1. In the spectrum of PPy, the peaks at 1557 cm^{-1} and 1476 cm^{-1} are attributed to the asymmetric and symmetric ring-stretching vibration of PPy, respectively^[15]. Meanwhile, the peaks at 3415 cm^{-1} , 1048 cm^{-1} and 1322 cm^{-1} are related to the N-H stretching vibration, C-H in-plane deformation vibration and C-N stretching vibration, respectively. In addition, strong peaks at 1202 cm^{-1} and 929 cm^{-1} indicate the doping state of PPy. For GO, the stronger C=O stretching vibration peak at 1626 cm^{-1} , and the C-O stretching vibration peak at 1060 cm^{-1} reveal that there exist oxygen-containing functional groups on the surface of the GO. The peak at 3440 cm^{-1} is attributed to hydroxyl group (-OH) on the surface of GO. However, the intention of GO characteristic peaks weaken greatly in the spectrum of rGO, ascribed to the fact that oxygen containing groups are reduced by vitamin C^[14]. Furthermore, all characteristic peaks of PPy could be found to blue shift in PPy/rGO-CTAB, suggesting that graphene layers were doped into the PPy backbone^[16].

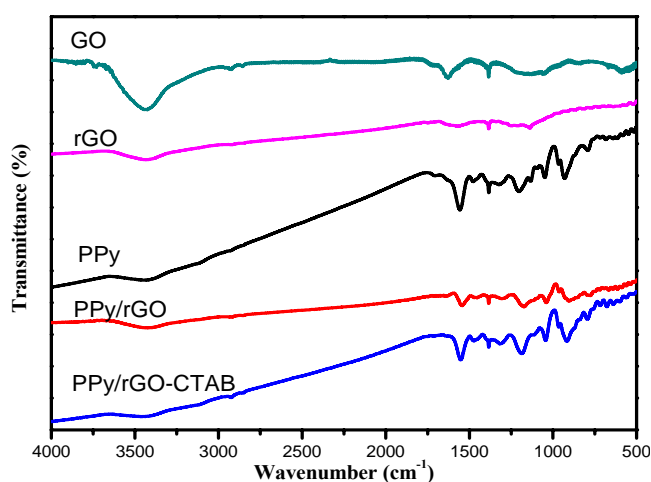


Fig. 1 FTIR spectra of GO, rGO, PPy, PPy/rGO and PPy/rGO-CTAB samples.

However, the differences of the intention and the position of the peaks for the composites could be observed, which demonstrates that oxygen-containing functional groups on the surface of GO are reduced by PPy^[17]. The FTIR results exhibit successful combination of both PPy and rGO.

3.3 Raman spectra analysis

The Raman spectra of GO, rGO, PPy, PPy/rGO and PPy/rGO-CTAB are shown in Fig.2.

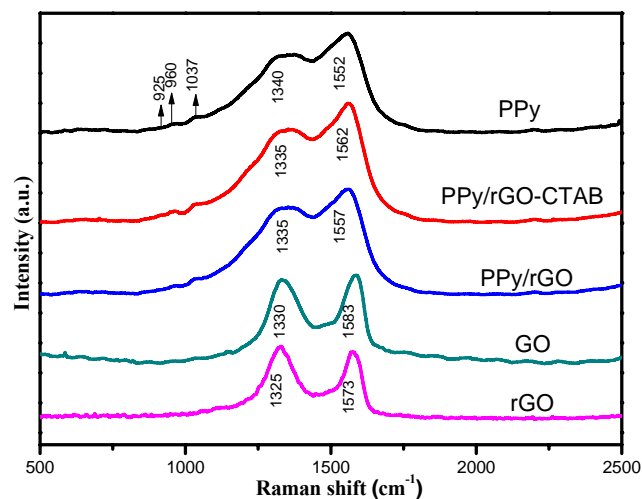


Fig. 2 Raman spectra of GO, rGO, PPy, PPy/rGO and PPy/rGO-CTAB samples.

In the spectra of GO and rGO, the peaks located at about 1330 cm^{-1} and 1580 cm^{-1} are related to D bands and G bands, respectively^[18]. The D bands are ascribed to the K-point phonons of A_{1g} symmetry resulted from the vibration of aromatic rings, corresponding to edges and structure defect. And the G bands represent first-order scattering of the E_{2g} vibration mode, attributed to the vibration of sp^2 -bonded carbon. Moreover, the intensity ratio between D bands and G bands reflects the extent of disorder^[19]. The ratio of rGO is slightly higher than that of GO, which indicates higher extent of disorder for rGO, probably resulting from the exist of unrepairable defect residually and a decrease in the average size of the sp^2 domains after reduction by vitamin C^[20]. In the spectrum of PPy, the peaks at 1552 cm^{-1} and 1340 cm^{-1} arise from the π conjugated structure and ring stretching mode of polymer backbone, respectively^[21]. The peak at 1037 cm^{-1} can be ascribed to the C-H in-plane deformation, and the two faint peaks at 925 cm^{-1} and 960 cm^{-1} correspond to ring deformation of the quinoid polaronic and bipolaronic structure, respectively. The spectra of PPy/rGO and PPy/rGO-CTAB show the characteristic peaks of PPy, whereas the intensity of the G bands at 1562 cm^{-1} for PPy/rGO-CTAB is enhanced, which indicates the interaction between PPy and rGO-CTAB sheets^[22]. These results are consistent with the FTIR results.

3.4 XRD study

The XRD patterns of GO, rGO, PPy, PPy/rGO and PPy/rGO-CTAB are shown in Fig.3. It could be seen that GO displays an obvious sharp peak at 11.2° , which is related to an interlayer spacing of 0.68 nm in the GO. After reduction by vitamin C, rGO shows a

peak at 12.6° , a relative sharp peak at 24.8° and a weakened peak at 42.5° , which may be due to the fact that GO is not reduced completely by vitamin C and partial graphene stacks into graphite again in the process of drying. However, these peaks disappear in PPy/rGO and PPy/rGO-CTAB composites. The characteristic broad peak of PPy ascribed to the amorphous nature appears at 26° ^[23], and similar peaks can be discovered in PPy/rGO and PPy/rGO-CTAB composites. The results indicate that PPy and rGO have been completely incorporated together^[24]. Compared to PPy/rGO, the intensity of the peak at 26° in PPy/rGO-CTAB increases, which is ascribed to the higher content of rGO in composites because of the reduction of the surface tension and surface energy of GO-CTAB.

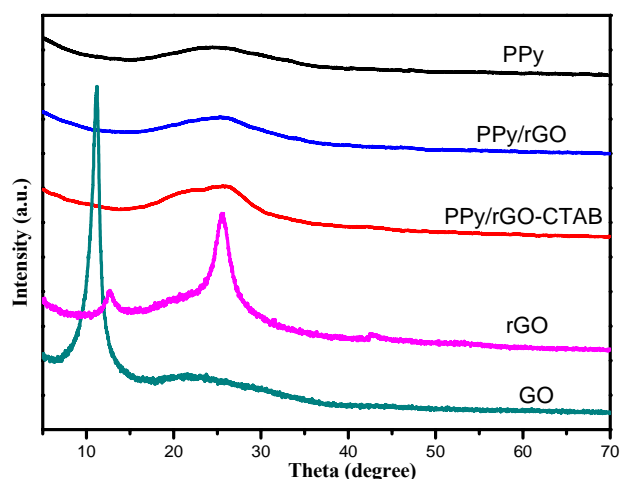


Fig. 3 XRD patterns of GO, rGO, PPy, PPy/rGO and PPy/rGO-CTAB.

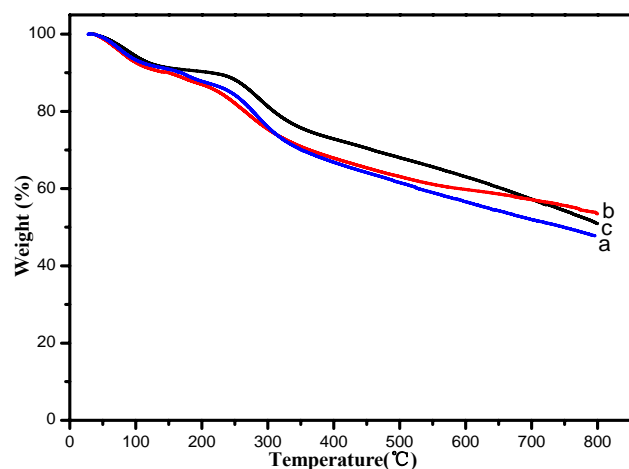


Fig. 4 TGA curves of (a) PPy, (b) PPy/rGO and (c) PPy/rGO-CTAB.

3.5 TGA investigation

TGA can be used to analyze the interaction between rGO and PPy, and to investigate the thermal stability of composites. As shown in Fig. 4, the slightly initial weight loss for all samples at the temperature of 100°C arises from the transpiration of water. At 250°C , all samples display a steep weight loss, which results from the degradation of PPy. At 800°C , both PPy/rGO with 53.45% weight retention and PPy/rGO-CTAB with 50.92% are higher than PPy with

47.77%, suggesting the enhanced thermal stability after the addition of rGO. Compared to PPy/rGO, PPy/rGO-CTAB possesses higher initial and maximum decomposition temperature due to stronger intermolecular force PPy and GO-CTAB as stated in section 3.1.

3.6 Morphological investigation

The SEM images of PPy, PPy/rGO and PPy/rGO-CTAB composites are shown in Fig. 5.

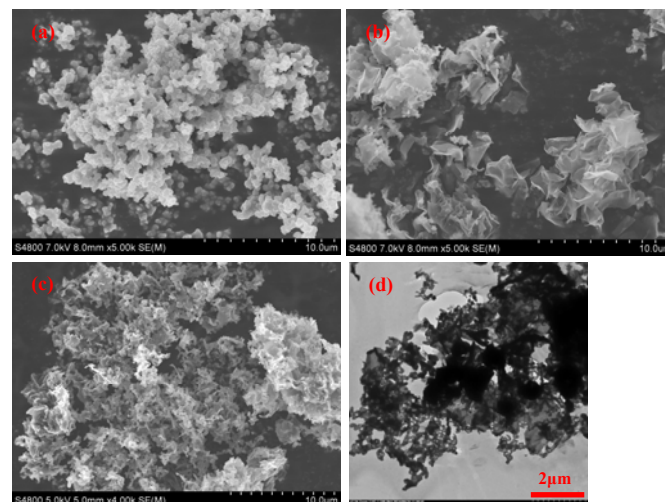


Fig. 5 The SEM images of (a) PPy, (b) PPy/rGO, (c) PPy/rGO-CTAB samples, and TEM of (d) PPy/rGO-CTAB.

The pure PPy (Fig. 5a) shows obvious spherical nano-particle. For PPy/rGO composite (Fig. 5b), the rGO with thin layers could be observed, unfortunately, tiny PPy is nonuniformly polymerized on the surface of rGO nanosheets. Compared with PPy/rGO composite, the morphology of PPy/rGO-CTAB composite (Fig. 5c) shows that the chain-structure PPy is coated on the surface of rGO densely and uniformly, which may be due to the stronger intermolecular force between pyrrole and GO-CTAB and lower surface tension and surface energy of GO-CTAB before the polymerization of pyrrole monomers under the initiation of APS. It also can be seen from the TEM image of PPy/rGO-CTAB composite (Fig. 5d), the rGO with few layers exhibits gauze-like morphology and the chain-structure PPy inserts into the interlayers between the rGO sheets, which could hinder the agglomeration of rGO and increase the specific surface area. In addition, the chain-structure PPy provides a convenient pathway for electrolyte ion to internal pore of electrode.

3.7 Electrochemical properties

3.7.1 Cyclic voltammetry (CV) study

Figure 6 shows the CV curves of rGO, PPy, PPy/rGO and PPy/rGO-CTAB composites tested at the scan rate of 5 mV/s in the three electrode system within an aqueous $1\text{ M H}_2\text{SO}_4$ electrolyte. In the CV curves, the scanning voltage couldn't be more than 0.5 V when saturated calomel electrode (SCE) is used as reference electrode. Otherwise oxidative degradation would happen in the P-doping PPy chains, reducing the electrochemical activity and the electrical conductivity of materials^[25]. The CV curve of rGO shows a nearly rectangular shape, and a pair of peaks (0.3 V) due to the

faradaic process caused by oxygen-containing groups residually^[26]. In the CV curve of PPy, a pair of redox peaks (-0.2 to 0.2V) attributed to the transformation between oxidation state and reduction state reveals the pseudocapacitance behavior of PPy. Such similar redox peaks could be observed in the CV curves of both PPy/rGO and PPy/rGO-CTAB composites, which demonstrates that the composites contain intact PPy molecular.

The area of CV curve is related to the capacitance. As shown in Fig. 6, the areas of both PPy/rGO and PPy/rGO-CTAB composites are larger than those of both rGO and PPy, indicating that composites possess much higher capacitance. And the area of PPy/rGO-CTAB composite is the largest owing to synergistic effect of rGO and PPy. On the one hand, the rGO could be served as skeleton for polymerization of pyrrole, improving the mechanical property and electrical conductivity of composites. On the other hand, the dense and uniform chain-structure PPy's formed on the surface of rGO, impede the stack of rGO nanosheets and enlarge the interlayer spaces of graphene, which devotes the high pseudocapacitance of the composite.

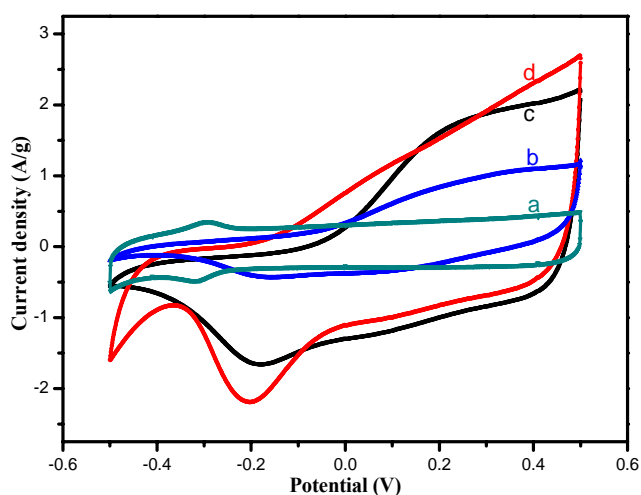


Fig. 6 The CV curves of (a) rGO, (b) PPy, (c) PPy/rGO and (d) PPy/rGO-CTAB at the scan rate of 5 mV/s.

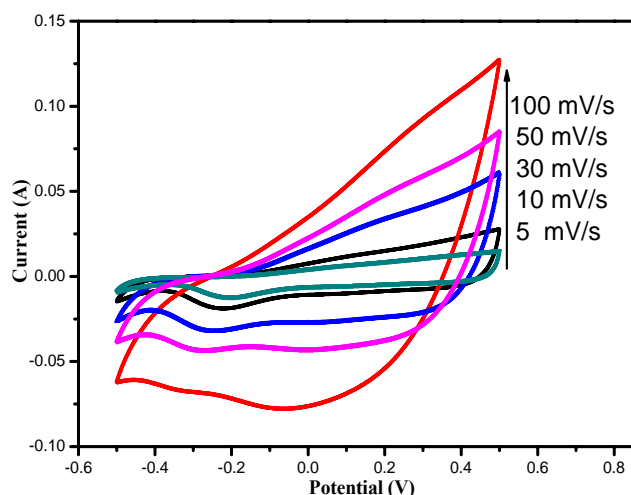


Fig. 7 The CV curves of PPy/rGO-CTAB at the different scan rate.

Figure 7 shows the CV curves of PPy/rGO-CTAB at different scan rate. The current increases with increasing potential scan rate, indicating fast response to oxidation/reduction on the current changes due to redox process^[27]. Due to the fact that electrolyte ion has not enough time to reach the inside of electrode in the fast electrochemical process, it is noted that the intensity of redox peaks is weakened gradually with increasing potential scan rate.

3.7.2 Galvanostatic charge-discharge (GCD) study

It can be found from Fig. 8, the GCD curves of PPy, PPy/rGO and PPy/rGO-CTAB samples at the constant charge and discharge current density of 0.5 A/g display irregular triangular shape, suggesting that the capacitance originates from pseudocapacitance. The capacitance could be evaluated by the discharge time according to equation (1). The discharge time of PPy/rGO-CTAB is longer than those of rGO, PPy and PPy/rGO, which demonstrates that the specific capacitance of PPy/rGO-CTAB is the largest among these samples. The PPy/rGO-CTAB sample has specific capacitance of 324.8 F/g, which is higher than 224.6 F/g of PPy/rGO, 170.3 F/g of PPy and 40.1 F/g of rGO.

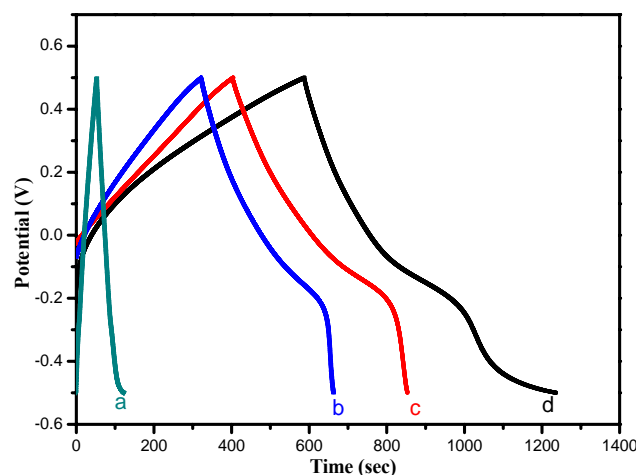


Fig. 8 The GCD curves of (a) rGO, (b) PPy, (c) PPy/rGO and (d) PPy/rGO-CTAB at current density of 0.5 A/g.

Meanwhile, the ohmic drop could be observed from all the GCD curves, which is attributed to the internal resistance at the beginning of discharge stage. The ohmic drop of PPy/rGO-CTAB sample is relatively smaller, implying smaller internal resistance.

The higher specific capacitance and smaller internal resistance of PPy/rGO-CTAB composite might be put down to the reasonable synthetic approach, well designed structure and the synergistic effect of PPy and rGO. The chain-structure PPy's formed on the surface of rGO not only prevent the agglomeration of rGO nanosheets because of the enlarged interlayer spaces of rGO in the existence of CTAB, but also offer electrolyte ions a convenient pathway to inside pore of electrode materials. Furthermore, as discussed above, the PPy/rGO-CTAB composites hold both good conductivity property of rGO and high pseudocapacitance of PPy.

Figure 9 shows the GCD curves of PPy/rGO-CTAB at different charge and discharge current density. When the current densities are 5 A/g, 2 A/g, 1 A/g and 0.5 A/g, corresponding specific capacitances are 147.1 F/g, 207.1 F/g, 257.2 F/g and 324.8 F/g respectively. With

the decrease of the current density, the discharge time increases, nevertheless, the ohmic drop reduces gradually. It could be attributed to the efficient access to inner surface of electrode materials for electrolyte ion in the electrochemical process, where the redox reaction occurs adequately^[28].

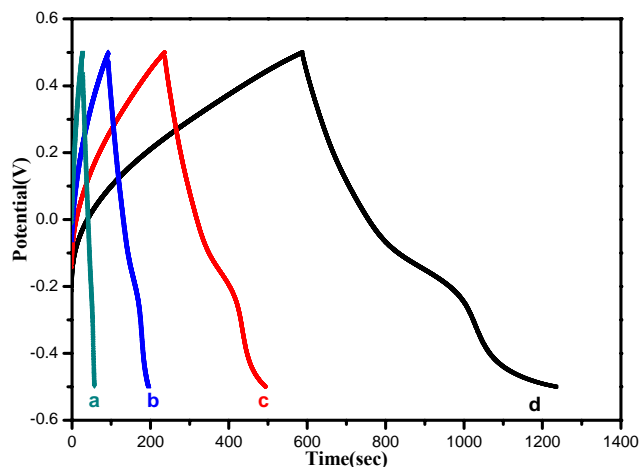


Fig. 9 The GCD curves of PPy/rGO-CTAB composite at different current density: (a) 5 A/g, (b) 2 A/g, (c) 1 A/g and (d) 0.5 A/g.

3.7.3 Electrochemical impedance spectroscopy (EIS) study

Fig. 10 shows the EIS curves of rGO, PPy, PPy/rGO and PPy/rGO-CTAB samples.

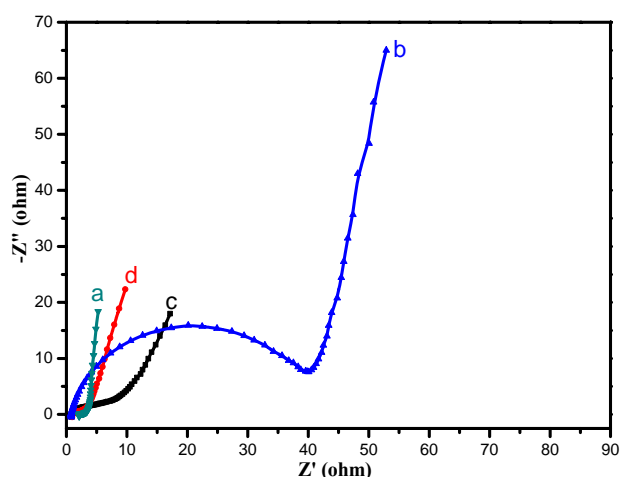


Fig. 10 EIS curves of (a) rGO, (b) PPy, (c) PPy/rGO and (d) PPy/rGO-CTAB samples.

The EIS data are analyzed via Nyquist plots which consist of two sections: a semi-circle at high frequency range and a linear slope at low frequency range. At high frequency range, large semi-circle reflects the high charge transfer resistance attributed to the poor electrical conductivity of samples, and the intercept at Z' along X-axis indicates the equivalent series resistance (ESR)^[29]. All samples exhibit small ESR at about 1 ohm. Compared to PPy with the largest semi-circle which is indicative of the poorest electrical conductivity, PPy/rGO-CTAB composites display much relative higher electrical conductivity attributed to the addition of rGO. At low frequency

range, the more vertical line indicates a cell more closing to an ideal capacitor. Meanwhile, due to the frequency dependence of ion diffusion/transport in the electrolyte, the Warburg resistance is presented in the 45° slope line^[30]. The larger Warburg region reflects longer diffusion path length of ions and increases obstruction of ion movement. From the Nyquist plots, PPy/rGO-CTAB displays much shorter ions diffusion path length than PPy, which is consistent with the results obtained in the GCD analysis.

3.7.4 Cyclic stability study

The cyclic stability of the rGO, PPy, PPy/rGO and PPy/rGO-CTAB electrodes was measured by cyclic voltammograms at the scan rate of 50 mV/s and shown in Fig. 11. It could be observed from Fig. 11 that the capacitance retention of pure PPy keeps only 52% after 500 cycles. The fact may be attributed to the degradation of PPy chains which is caused by the swelling/shrinkage of polymer chains during doping and de-doping process, and engenders small soluble oligomers, resulting in a great mass loss of PPy^[31]. However, after the addition of rGO, the capacitance retention ratios of PPy/rGO and PPy/rGO-CTAB rise to 56% and 64% respectively, which originates from the fact that rGO could enhance the mechanical strength of the composite materials efficiently. Besides, compared with PPy/rGO, PPy/rGO-CTAB displays better cyclic stability, which may be due to the stronger intermolecular force between pyrrole and GO-CTAB and lower surface tension and surface energy of GO-CTAB before polymerization of pyrrole monomers under the initiation of APS.

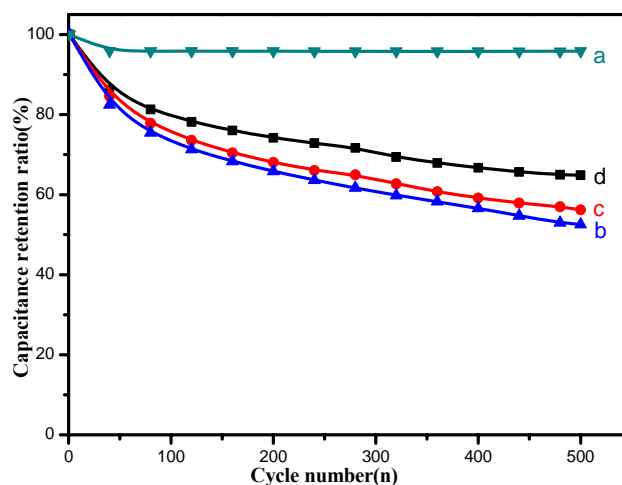


Fig. 11 Capacitance retention ratios of (a) rGO, (b) PPy, (c) PPy/rGO and (d) PPy/rGO-CTAB tested at the scan rate of 50 mV/s

4 Conclusions

In summary, we utilized a renewable and efficient method to synthesize hierarchical nanostructured PPy/rGO composites for electrode materials of supercapacitor. The dense and uniform PPy chains formed on the surface of GO modified by CTAB, could hold back the agglomeration of rGO in composites efficiently. Due to the hierarchical nanostructure in PPy/rGO-CTAB composites, which might offer a convenient pathway to internal pore of electrode materials for electrolyte ions, PPy/rGO-CTAB composites possessed better thermal stability, higher specific capacitance, lower resistance,

relatively higher cyclic property and faster response to oxidation/reduction than both PPy/rGO composites without addition of CTAB and rGO. The specific capacitance of PPy/rGO-CTAB was 324.8 F/g at the current density of 0.5 A/g.

Acknowledgements

The authors acknowledge the financial support of National Natural Science Foundation of China (51363005), the Scientific Foundation of Colleges and Universities of Guangxi Province (2013YB115), the Innovation Project of Guangxi Graduate Education (YCSZ2013076), and the Guangxi Funds for Specially-appointed Expert, and the Guangxi Small Highland Innovation Team of Talents in Colleges and Universities. The authors express their deep sense of gratitude to Dr. Weixing Deng and Prof. Wenfeng Zhu (College of Materials Science & Engineering, Guilin University of Technology) for SEM and TEM characterizations, respectively.

Notes and references

Key Laboratory of New Processing Technology for Nonferrous Metals and Materials, Ministry of Education, College of Materials Science & Engineering, Guilin University of Technology, Guilin 541004, P.R. China

- [1] Y. Zhu, S. Murali, M.D. Stoller, et al. *Science*, 2011, 332(6037): 1537-1541.
- [2] R. Kötz, M. Carlen. *Electrochim. Acta*, 2000, 45(15): 2483-2498.
- [3] A.K. Geim, K.S. Novoselov. *Nat. Mater.*, 2007, 6(3): 183-191.
- [4] G. Wang, L. Zhang, J. Zhang. *Chem. Soc. Rev.*, 2012, 41(2): 797-828.
- [5] M Wu, P Ai, M Tan, et al. *Chem. Eng. J.*, 2014, 245: 166-172.
- [6] J. Zhang, X.S. Zhao. *The J. Phys. Chem. C*, 2012, 116(9): 5420-5426.
- [7] Y. Liu, Y. Zhang, G. Ma, et al. *Electrochim. Acta*, 2013, 88: 519-525.
- [8] I.M.D.F. Salas, Y.N. Sudhakar, M. Selvakumar. *Appl. Surf. Sci.*, 2014, 296: 195-203.
- [9] C. Xu, J. Sun, L. Gao. *J. Mater. Chem.*, 2011, 21(30): 11253-11258.
- [10] Y. Fan, Y. Liu, Q. Cai, et al. *Synth. Met.*, 2012, 162(21): 1815-1821.
- [11] S. Biswas, L.T. Drzal. *Chem. Mater.*, 2010, 22(20): 5667-5671.
- [12] D.C. Marcano, D.V. Kosynkin, J.M. Berlin, et al. *ACS Nano*, 2010, 4(8): 4806-4814.
- [13] X. Zhang, J. Zhang, Z. Liu, et al. *Chem. Commun.*, 2004 (16): 1852-1853.
- [14] J. Zhang, H. Yang, G. Shen, et al. *Chem. Commun.*, 2010, 46(7): 1112-1114.
- [15] G. Cho, B.M. Fung, D.T. Glatzhofer, et al. *Langmuir*, 2001, 17(2): 456-461.
- [16] H. Wang, Q. Hao, X. Yang, et al. *Electrochem. Commun.*, 2009, 11(6): 1158-1161.
- [17] S. Bose, T. Kuila, A.K. Mishra, et al. *J. Mater. Chem.*, 2012, 22(19): 9696-9703.
- [18] C. Bora, S.K. Dolui. *Polym. Int.*, 2013, 63(8): 1439-1446.
- [19] K.N. Kudin, B. Ozbas, H.C. Schniepp, et al. *Nano Lett.*, 2008, 8(1): 36-41.
- [20] S. Stankovich, D.A. Dikin, R.D. Piner, et al. *Carbon*, 2007, 45(7): 1558-1565.
- [21] S. Biswas, L.T. Drzal. *Chem. Mater.*, 2010, 22(20): 5667-5671.
- [22] V. Chandra, K.S. Kim. *Chem. Commun.*, 2011, 47(13): 3942-3944.
- [23] A. Liu, C. Li, H. Bai, et al. *J. Phys. Chem. C*, 2010, 114(51): 22783-22789.
- [24] Y. Fan, Y. Liu, Q. Cai, et al. *Synth. Met.*, 2012, 162(21): 1815-1821.
- [25] Y. Li, R. Qian. *Electrochim. Acta*, 2000, 45(11): 1727-1731.
- [26] Y.R. Nian, H. Teng. *J. Electrochem. Soc.*, 2002, 149(8): A1008-A1014.
- [27] H.W. Park, T. Kim, J. Huh, et al. *ACS Nano*, 2012, 6(9): 7624-7633.
- [28] W Wan, L Li, Z Zhao, et al. *Adv. Funct. Mater.*, 2014, 24(31): 4915-4921.
- [29] D. Xu, Q. Xu, K. Wang, et al. *ACS Appl. Mater. Inter.*, 2013, 6(1): 200-209.
- [30] K. Zhang, L.L. Zhang, X.S. Zhao, et al. *Chem. Mater.*, 2010, 22(4): 1392-1401.
- [31] Q. Fu., B. Gao., H. Dou, et al. *Synth. Met.* 2011, 161(5), 373-378.